REPORT DOCUMENTATION PAGE

Form Approved
OMB No. 0704-0188

1. AGENCY USE ONLY (Leave blank)	2. REPORT DATE	3. REPORT TYPE AND DATES COVERED
	April 1998	mar 1 97-Sept 30 98

4. TITLE AND SUBTITLE
3D multi-valued traveltime and amplitude maps

5. FUNDING NUMBERS
N0001-95-0508
PR:21aa188---01

6. AUTHOR(S)
Lan Wang and Norman Bleistein

7. PERFORMING ORGANIZATION NAME(S) AND ADDRESS(ES)
Center for Wave Phenomena
Colorado School of Mines
Golden, CO 80401

8. PERFORMING ORGANIZATION REPORT NUMBER
CWP-278

9. SPONSORING/MONITORING AGENCY NAME(S) AND ADDRESS(ES)
Ocean Acoustics Division
800 N. Quincy St.
Arlington, VA 22217-5660

10. SPONSORING/MONITORING AGENCY REPORT NUMBER

11. SUPPLEMENTARY NOTES

12b. DISTRIBUTION CODE

DISTRIBUTION STATEMENT A
Approved for public release;
Distribution Unlimited

Ray theorectic modeling with stable and accurate amplitude requires a velocity model that has a continuous first derviative. After studying alternatives, we concluded that a standard smoothed physical model on a Cartesian grid is likely to lead to a computer code of competitive cpu speed, when amplitude accuracy is of as much concern as traveltime accuracy. We use a wave front construction technique, in which the size of triangular plates connecting three nearby rays on the isochron (surface of constant traveltime) are used as an indicator of adequate density of rays. When the criteria for density of rays are violated, data at new points on the wavefront are interpolated into the family of rays and the wavefront construction continues. In this manner, the method does not require excessing density of rays at small traveltimes in order to maintain adequate density of rays at larger traveltimes. The technique

14. SUBJECT TERMS	15. NUMBER OF PAGES
amplitude, dynamic ray tracing, analytic ray tracing wavefront construction	9
	16. PRICE CODE

17. SECURITY CLASSIFICATION OF REPORT	18. SECURITY CLASSIFICATION OF THIS PAGE	19. SECURITY CLASSIFICATION OF ABSTRACT	20. LIMITATION OF ABSTRACT

NSN 7540-01-280-5500

Standard Form 298 (Rev. 2-89)
Prescribed by ANSI Std 239-18
298-102

ONR/OA
N00014-95-1-0508
CWP-278
May 1998

3D multi-valued traveltime and amplitude maps

Lan Wang & Norman Bleistein

This paper was presented at the Annual CWP Project Review Meeting,
May 11-15, 1998, Vail Colorado.

Center for Wave Phenomena
Colorado School of Mines
Golden, Colorado 80401
(303)273-3557

3D multi-valued traveltime and amplitude maps

Lan Wang & Norman Bleistein

ABSTRACT

Ray-theoretic modeling requires accurate amplitude as well as phase both for forward modeling and Kirchhoff inversion, among other applications. There are no analytical solutions to the ray equations in realistic earth models, thus, we must use numerical solutions to solve problems of interest. For three dimensional applications, it is a challenge to develop numerical modeling codes that require reasonable cpu time while achieving sufficient amplitude accuracy to be useful in applications.

For the case of linear sloth (slowness squared or inverse wavespeed squared), analytical solutions of the ray equations *do* exist, leading to a combined numerical analytical technique. In this method, the physical model is decomposed into tetrahedral blocks of sufficiently small size to allow for the linear sloth approximation to be valid in each. Analytical solutions in each tetrahedron are then pieced together to provide global solutions. The ray tracing with this method is relatively fast. However, the wavespeed model generated by this technique is not sufficiently smooth to produce accurate amplitudes, numerically. Recent attempts to further smooth the physical model defeat the advantage of speed of the algorithm because the smoothness conditions across the faces of the tetrahedra generate a coupled system of equations of a size proportional to the number of tetrahedra in the global physical model. This is not practical in $3D$. Thus, we conclude that a standard smoothed physical model on a Cartesian grid is likely to lead to a computer code of competitive cpu speed, when amplitude accuracy—dynamics—is of as much concern as traveltime accuracy—kinematics.

In either case, we use a *wavefront construction* technique, in which the size of triangular plates connecting three nearby rays on the isochron (surface of constant traveltime) is used as an indicator of adequate density of rays. When the criteria for density of rays are violated, data at new points on the wavefront are interpolated into the family of rays and the wavefront construction continues. In this manner, the method does not require excessive density of rays at small traveltimes in order to maintain adequate density of rays at larger traveltimes. The technique allows for multi-pathing (caustics) and for amplitude propagation along each of the branches of the wavefront.

Applications of the modeling technique are shown.

Key words: amplitude, dynamic ray tracing, analytic ray tracing, wavefront construction

Introduction

In this report, we address the problem of accurate and efficient determination of multi-valued $3D$ maps for amplitude as well as traveltimes or any other ray-related variables throughout the target zone from any shot and receiver position. The current interest in $3D$ seismic imaging has considerably increased the importance of ray tracing methods in wave field computations. Among seismic modeling methods, ray tracing methods provide a reasonable compromise between ac-

curacy and computational efficiency. For the computation of traveltime, various methods have been described. Among those, the finite-differencing (FD) method, i.e., FD-solvers of the eikonal equation, has recently become a popular method for calculation of "first arrival" traveltimes (Vidale, 1988). However, this method suffers from the disadvantages that it is restricted to the computation of first arrivals only and it produces unreliable amplitudes. Both are severe disadvantages for Kichhoff-type algorithms, such as the Bleistein/Cohen inversion (Bleistein *et al.*, 1987; Bleistein *et al.*, 1996), where the calculation of amplitudes is necessary to determine the weighting factor in inhomogeneous media. Furthermore, in complex media, such as near salt domes and in sub-salt regions, later arrival traveltimes should be considered to obtain better image quality. Amplitudes can be used, among other things, to find most energetic arrivals.

Simultaneous computation of traveltimes and amplitudes is possible by dynamic ray tracing (DRT). It provides accurate multiple arrivals, amplitude and phase. Estimation of these ray data can be carried out either by numerical solution of ray tracing equations in general smooth grid-based models or by piecewise analytic solutions for certain simple velocity functions in tetrahedral models. Among the choices of ray tracing procedures, the simplest and fastest solution of the ray tracing system is usually based on its analytic solution, wherever the complexity of the model allows one. This is usually referred to as analytic ray tracing or cell ray tracing. Generally, the whole medium is divided into suitable cells (usually tetrahedra in $3D$), in which the velocity can be approximated by simple functions that permit analytic ray solutions. The ray in the whole model is then obtained as a chain of analytically computed segments. The analytic ray tracing is usually performed for models in which either the velocity, $v(x_i)$, or $1/v(x_i)$, or $1/v^2(x_i)$, is a linear function of Cartesian coordinates. The simplest analytic solution for inhomogeneous medium is the one for constant gradient of squared slowness, also referred as linear sloth media (Červený, 1987; Meng & Bleistein, 1997). However, this assumption leads to tetrahedral cells with artificial second-order discontinuities at their interfaces. As a consequence, this approach produces unreliable amplitude coefficients across the internal boundaries. Körnig (1995) proposed a method using quadratic sloth. In this approach, the squared slowness and its gradient with respect to spatial variables are continuous across each cell boundary. The analytic solutions for such a velocity function are determined by using Laplace transform. Also, the computation of amplitude can be largely simplified by calculating the ray Jacobian directly from the analytical ray equations. However, the problem of determining the cell constants in quadratic sloth is rather difficult. The model design leads to a huge matrix inversion problem, and is impractical in $3D$. Only $2D$ implementation of the traveltime computation was carried out by Körnig (1995). We have concluded that the analytic approach in tetrahedral cells does not likely offer efficient algorithms in dynamic applications.

Traditionally, numerical DRT is performed by shooting a fan of rays from the source and extrapolating traveltimes and amplitude away from the rays into their nearby regions (Červený, 1987; Virieux & Farra, 1991; Sun & Biondi, 1995). The main disadvantage of the conventional shooting method is the lack of control of ray density in the search fan. Therefore, it is hard to reach a favorable compromise between efficiency and reliability, especially in complex $3D$ models. It also produces shadow zones in areas of large velocity contrasts. The wavefront construction traveltime computation method (Vinje *et al.*, 1996) offers a solution to this problem by dynamically adding rays as needed. In this method, rays are maintained by a triangular network, and are traced stepwise in traveltime through the model. The wavefronts are then obtained automatically as a by-product of the ray tracing. In this report, the idea of wavefront construction is applied to $3D$ complex models for estimation of both traveltime and amplitude coefficients. The dynamic interpolation of new rays assures that the wavefront is equipped with sufficient ray density at each computational step. Linear interpolation of traveltime with respect to the simulated wavefronts and linear interpolation of amplitude in terms of tube cross sectional area are performed at grid points that fall into the subvolume formed by every two successive wavefronts. A grid point can be passed by different sequences of wavefronts and, thereby, multi-valued arrivals can be detected and recorded. In this manner, all the grid points in the model are equipped with accurate—perhaps multivalued—traveltimes and amplitudes.

In the following sections, we first discuss the possibility of applying analytic solutions in tetrahedral models for amplitude estimation. Thereafter, we address some important issues in numerical DRT such as interpolation of new rays and estimation of parameters at grid points. We also propose a smooth gridded model representation for the purpose of computational efficiency. Finally, we show results of applying this method to different velocity models.

Dynamic ray tracing

This section is a brief review of the dynamic ray tracing theory, based on Červený (1987), (1995). We begin by introducing two coordinate systems involved in

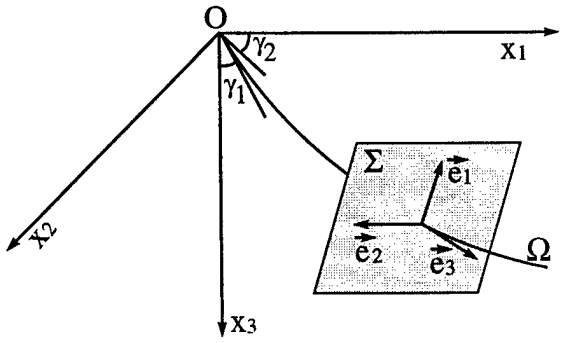

Figure 1. The ray-centered coordinate system. $\vec{e_3}$ is tangent to the ray path Ω. $\vec{e_1}$ and $\vec{e_2}$ form a plane perpendicular to $\vec{e_3}$. γ_1 and γ_2 are the ray parameters that specify the ray, usually they are either the take-off angles(shown in this figure) or the slowness vector components at the source.

DRT — the ray-centered coordinate system and the ray parameter coordinate system.

The ray-centered coordinate system, denoted by (q_1, q_2, q_3), is a curvilinear orthogonal coordinate system associated with any selected ray Ω (see Fig 1). One coordinate, say q_3, corresponds to any monotonic parameter along the ray, such as the arc length s, the traveltime τ or the parameter σ, with $d\tau = d\sigma/v^2$. Here, we take $q_3 = \tau$, the traveltime of ray Ω away from the source. Thus, the traveltime, itself, is one of the coordinate axes in the ray-centered coordinate system. Coordinates q_1 and q_2 form a $2D$ Cartesian coordinate system in the plane Σ perpendicular to Ω at $q_3 = \tau$, with the origin at Ω. The vector basis of the ray-centered coordinate system connected with Ω is formed at any arbitrary point $q_3 = \tau$ of ray Ω by a right-handed triplet of unit vectors $\vec{e_1}(\tau), \vec{e_2}(\tau), \vec{e_3}(\tau)$, as shown in Fig 1. Unit vectors $\vec{e_i}(\tau)$ can also be viewed as polarization vectors for isotropic media. The unit vector $\vec{e_3}$ determines the direction of the displacement vector of P waves, which is always linearly polarized. Especially important are unit vectors $\vec{e_1}, \vec{e_2}$, since they determine the polarization of S waves, when we are dealing with vector solutions of the elastic wave equation.

The ray parameter coordinates, $(\gamma_1, \gamma_2, \gamma_3)$, are defined as following: γ_1 and γ_2 are the ray parameters that specify the ray, usually they are either the take-off angles or the slowness vector components at the source; γ_3 is any monotonic parameter along the ray, s, τ or σ. The Jacobian J of transformation from ray coordinates, $(\gamma_1, \gamma_2, \gamma_3)$, to the general Cartesian coordinates, (x_1, x_2, x_3), is an important factor in computation of the ray amplitude (Bleistein, 1984). The ray amplitude has the following form,

$$A(\mathbf{x}, \mathbf{x_0}) = \frac{const}{\sqrt{|J|}}, \tag{1}$$

with,

$$J = \det\left[\frac{\partial(x_1, x_2, x_3)}{\partial(\gamma_1, \gamma_2, \gamma_3)}\right]. \tag{2}$$

Here, $A(\mathbf{x}, \mathbf{x_0})$ is the amplitude at $\mathbf{x} = (x_1, x_2, x_3)$ corresponding to the source $\mathbf{x_0} = (x_{10}, x_{20}, x_{30})$; J is the Jacobian; and the constant is determined by the choice of $(\gamma_1, \gamma_2, \gamma_3)$.

The rays are defined as the characteristics of the eikonal equation. That is, by transforming the eikonal equation to the following six ray equation by using the method of characteristic, (Bleistein, 1984)

$$\begin{aligned} \frac{dx_i}{d\tau} &= v^2 p_i, \\ \frac{dp_i}{d\tau} &= -\frac{1}{v}\frac{\partial v}{\partial x_i}, \qquad i = 1, 2, 3. \end{aligned} \tag{3}$$

Here, $x_i(\tau)$ denotes the coordinates of position along the ray, $p_i(\tau)$ denotes the components of the slowness vector, τ denotes the traveltime along the ray, and $v(x_i)$ denotes the velocity. System (3) is often referred as the kinematic ray tracing (KRT) system.

Differentiating the KRT system (3) with respect to the ray coordinates γ_i and applying Taylor approximation up to second-order in q_i will generate the dynamic ray tracing system. The DRT system can be expressed in many forms and in various coordinate systems. The simplest form of the DRT system is obtained in ray-centered coordinates connected with the ray Ω:

$$\begin{aligned} \frac{d\mathbf{Q}}{d\tau} &= v^2 \mathbf{P}, \\ \frac{d\mathbf{P}}{d\tau} &= -\frac{1}{v}\mathbf{V}\mathbf{Q}, \end{aligned} \tag{4}$$

where $\mathbf{Q}$, $\mathbf{P}$ and $\mathbf{V}$ are 2×2 matrices defined as

$$\begin{aligned} Q_{ij} &= \frac{\partial q_i}{\partial \gamma_j}, \qquad i, j = 1, 2, \\ P_{ij} &= \frac{\partial p_i}{\partial \gamma_j}, \qquad i, j = 1, 2, \\ V_{ij} &= \left.\frac{\partial^2 V(q_1, q_2, S)}{\partial q_i \partial q_j}\right|_{q_1 = q_2 = 0} \\ &= H_{kl} v_{,kl} H_{lj}, \qquad i, j = 1, 2, \\ H_{kl} &= \vec{i_k} \cdot \vec{e_l}. \end{aligned} \tag{5}$$

Here, $\vec{i_k}$ are the basis vectors in general Cartesian coordinates (x_1, x_2, x_3) and H is the transform matrix from (q_1, q_2, q_3) to (x_1, x_2, x_3), its element H_{kl} represents the

kth Cartesian component of basis vector $\vec{e_l}$. Elements V_{ij} of the matrix V are the second derivatives of velocity v with respect to q_i, and equivalent to the second derivatives with respect to x_i under transformation H. Therefore, dynamic ray tracing (4) requires continuity of the velocity field up to second derivatives.* $\mathbf{Q}$ is a transformation matrix from the ray parameters γ_1, γ_2 to the ray-centered coordinate q_1, q_2. Its determinant measures the ray Jacobian (2), and is also called the geometrical spreading factor. $\mathbf{P}$ is a transformation matrix from the ray parameters γ_1, γ_2 to the slowness vector component in the ray-centered coordinate system. The quantity $\mathbf{P}$ may also be defined by

$$\mathbf{P} = \frac{\mathbf{KQ}}{v} \tag{6}$$

where $\mathbf{K}$ is the wavefront curvature. The KRT system (3) computes the first derivatives of the traveltime field, while the DRT system (4) relates the second derivatives by the relationship,

$$\mathbf{M}(\tau) = \mathbf{PQ}^{-1}. \tag{7}$$

where $\mathbf{M}$ is 2×2 matrix $\mathbf{M}$ of second derivatives of the traveltime field with respect to the ray-centered coordinate q_1, q_2, $M_{i,j} = \partial^2\tau/\partial q_i \partial q_j$.

At caustic points, the ray Jacobian (2) or the determinant of matrix $\mathbf{Q}$ vanishes. In $3D$ structure, there are two kinds of caustic points depending on the range of the matrix. The ray tube may shrink to a caustic surface(envelope of rays) which is perpendicular to the direction of propagation (a caustic point of the first order); or the ray tube may shrink to a point (a caustic point of the second order). In passing through the caustic point of the first order, the ray Jacobian J changes sign and the argument of $J^{1/2}$ takes on the phase term $\pm\pi/2$. Similarly, in passing through the caustic point of the second order, the phase term is $\pm\pi$. The phase shift due to caustics is cumulative. If we pass through several caustic points along the ray, the total phase shift is the sum of the individual phase shifts, this is often referred as the KMAH amplitude.

Analytic ray tracing

It is known that the realistic velocity field of interest is often rather complicated and can hardly allow a general analytic solution of the ray tracing system. However, analytic ray tracing plays an important role in wave field computation. This is due, in part, because the analytic solutions are valuable in the cell approach, in which the whole model is subdivided into a set of tetrahedral cells with simple velocity functions within cells. The models allowing analytic solutions are usually those with either the velocity, or slowness, or squared slowness being a linear function of Cartesian coordinates. As we have mentioned before, this constraint does not provide enough smoothness for amplitude estimation. In this section, we discuss the analytic solutions for *quadratic sloth* media.

The quadratic sloth distribution, denoted by q, is defined as a quadratic function in space,

$$\begin{aligned} q(x_1, x_2, x_3) &= \frac{1}{v^2(x_1, x_2, x_3)} \\ &= A + 2B_i x_i + C_{ij} x_i x_j. \end{aligned} \tag{8}$$

The analytical solutions for this distribution were found by Körnig (1995) using the Laplace transform. In the Laplace domain, the ray coordinates, $X_i(s)$, are ratios of polynomials of sixth and seventh order, respectively, in s; this is the Laplace variable corresponding to σ, the ray tracing integral variable with $d\sigma = v^2 d\tau$. The expressions for the ray trajectories, $x_i(\sigma)$, can be obtained explicitly by inverse Laplace transform of $X_i(s)$ using partial fraction expansions. Depending on the distribution of eigenvalues of C_{ij}, the solutions of $x_i(\sigma)$ are generalized into seven different forms. For each case, the ray trajectories are in the general form

$$x_i(\sigma) = w_{ik} f_k(\sigma), \quad i = 1, 2, 3, \quad k = 1, 2, ..., 7. \tag{9}$$

Here, the w_{ik}'s are the weighting factors, which are functions of x_{i0}, p_{i0}, B_j and C_{ij} with x_{i0} and p_{i0} being the initial position and slowness components; $f_k(\sigma)$ are the basis functions corresponding to the inverse transform of the partial fraction expansions. One of them is unity, the others are either low-order polynomials in σ, or trigonometric, or hyperbolic function.

Now we propose an alternative to Körnig's (1995) approach to calculate the amplitudes along rays. Notice that the $f_k(\sigma)$'s in (9) are functions depending only on σ, and w_{ik}'s can be expressed in terms of x_{i0}, p_{i0}, and constants B_j and C_{ij}. Therefore, if we choose $\gamma_1 = p_{10}, \gamma_2 = p_{20}$ and $\gamma_3 = \sigma$ in (2), the ray Jacobian J can be calculated analytically,

$$\begin{aligned} J &= \det \begin{bmatrix} \frac{\partial w_{ik}}{\partial p_{10}} f_k(\sigma) \\ \frac{\partial w_{ik}}{\partial p_{20}} f_k(\sigma) \\ w_{ik} g_k(\sigma) \end{bmatrix} \\ &= \det\{J_{ijk} j_k(\sigma)\} \end{aligned} \tag{10}$$

with summation over the repeated index, k, and

* It is the numerical sampling across tetrahedral interfaces that causes amplitude instability when the second derivative is not continuous.

$$j_k(\sigma) = \begin{cases} f_k(\sigma), & i = 1,2 \\ g_k(\sigma), & i = 3. \end{cases} \tag{11}$$

The coefficients J_{ijk} can be expressed for all the seven cases in (9). Notice that expression (10) has taken the place of the DRT system (4), and it is less computationally costly than solving the eight integral equations in small time steps.

This approach of making quadratic sloth assumption in tetrahedral models has eliminated the smoothing procedure across the internal interfaces. However, the constants A, B_i and C_{ij} in (8) are usually not known in advance from the given physical model. They have to be determined from the discrete model. The assumption of quadratic sloth is equivalent to the continuity of both q and the gradient of q across the internal cell faces. Therefore, the 10 constants A, B_i and C_{ij} in one tetrahedron cannot be determined by the velocity values at its four apices only, but also depend on the values in the neighboring cells. Such a model design problem for all the tetrahedral cells leads to a huge inverse problem. If the whole model is divided into N cells, the size of the coupled system of equation is proportional to $10N$, making the computation very time consuming. Furthermore, this inverse system is not always solvable, or has solutions in a least squares sense, at best. This is impractical in $3D$ and considerably limits the applicability of this approach.

From the above discussion, we see that although the assumption of quadratic sloth in tetrahedral models provides accurate amplitudes, this assumption leads to a difficult and inefficient numerical problem for determining the cell constants. And this problem exists in all extensions to quadratic physical models, not particularly in a quadratic sloth model. We conclude that analytic ray tracing in tetrahedral models is not likely to give us an efficient module for dynamics, although it has its applications in traveltime calculations.

Wavefront construction on smooth gridded models

Here and below, we will focus on numerically solving (3) and (4) for smooth gridded models. We will apply the technique of wavefront construction (WFC) to both kinematics and dynamics.

In the wavefront construction method, a relatively sparse number of rays are shot initially. They differ from each other by the two take-off angles, and are extrapolated into the zone of interest by solving (3) and (4) numerically with appropriate initial conditions. Required accuracy of traveltime and amplitude can be approached by various standard numerical procedures, such as Runge-Kutta or predictor-corrector, for example. At any computational step, the wavefront is obtained as a by-product of the ray tracing. The wavefront is represented by triangular plates that connect every three neighboring ray endpoints on the WF. The nearby rays in $3D$ are then defined and organized by such a triangular mesh consisting of the internal ordering of connecting endpoints in each triangle and adjacent triangle(s) to each of its sides. The processes of checking, interpolating of new rays and estimating of grid point parameters (described below) are all performed within such a triangular network. Rays are added and the original triangle is subdivided into new triangles when certain criteria, restricting the size of the triangular plates, are violated. In this manner, the wavefront always has sufficient ray density without *a priori* estimation of the number of rays needed, or by imposing an excessive ray density on initiation. For complex $3D$ velocity models, the wavefront surface may be very complicated, folding in on itself at some parts, for example; however, no tears or holes in the interior of the surface are allowed. In this sense, the wavefront is complete. On the other hand, a grid point can be passed by different sequences of wavefronts; multivalued arrivals can then be estimated and distinguished by their initial take-off angles.

The most attractive advantage of the WFC method is that it is more efficient than the conventional ray tracing method. In addition, WFC gives better ray coverage, especially in areas of large geometrical spreading where conventional ray tracing may give no arrivals. Furthermore, compared to FD-solvers, the WFC method is not restricted to the calculation of only first arrivals. Amplitude and other ray theoretical quantities are also available. Thus, it meets the requirements for accurate modeling of amplitude as well as phase, a requirement for inversion as opposed to migration.

Ray interpolation

The wavefront construction method is largely dependent on the procedure of interpolation of the wavefront at each step. New ray endpoints must be added along the simulated wavefront and must have the propagation direction that the ray would have had if it had been shoot from the source. This section addresses an algorithm for this procedure.

Rays diverge and the wavefronts expand through the wave-field. When new ray endpoints are needed to keep a certain ray density on the wavefront, the whole triangular network will have to be reorganized. The criterion for this interpolation can be the area of triangles, which must not exceed a pre-specified limit, and/or the angle deviation of the slowness vectors of two adjacent rays, which cannot be too large. New rays are always added

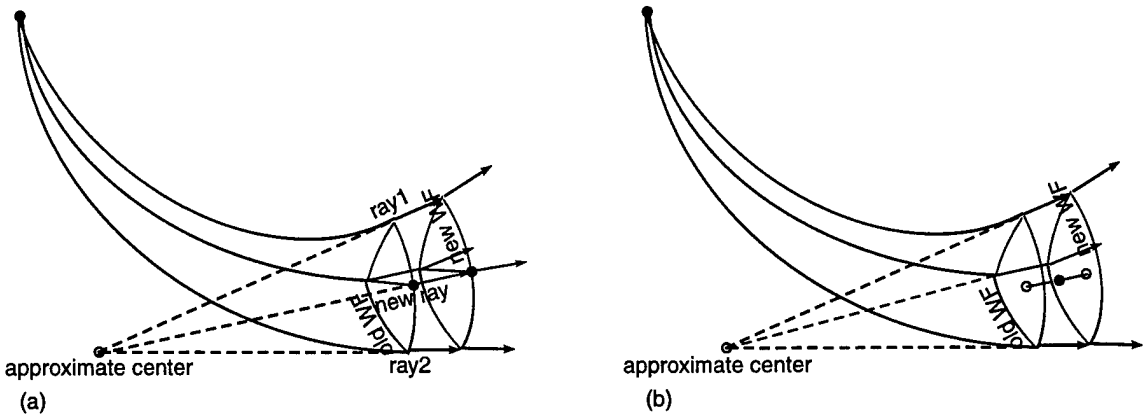

Figure 2. Interpolation of new rays and estimation of grid parameters are performed in a "ray tube". (a)Interpolation of a single new ray. The two ray endpoints and their propagation directions form two straight lines in $3D$. An "approximate" center can be defined as the midpoint of the line segment that connects the two straight lines at their points of shortest distance. This approximate center, along with the two ray ends at the old WF, form a fan and a circular curve connecting the two ray end points. The new ray position is then found along the dividing direction from the approximate center, and at its intersection with the circular curve. Then the interpolated ray is traced from the old to the new WF. (b)Simple ray cell with an interior grid point. Ray data are estimated with respected to the two simulated WFs.

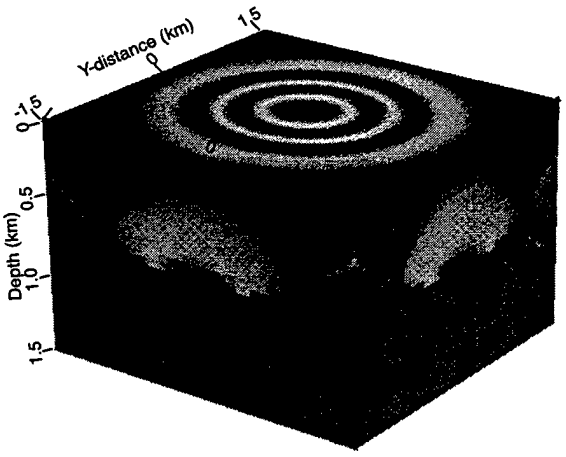

Figure 3. $3D$ wave field of a linear sloth model using WF construction method. The grey part is the shadow zone.

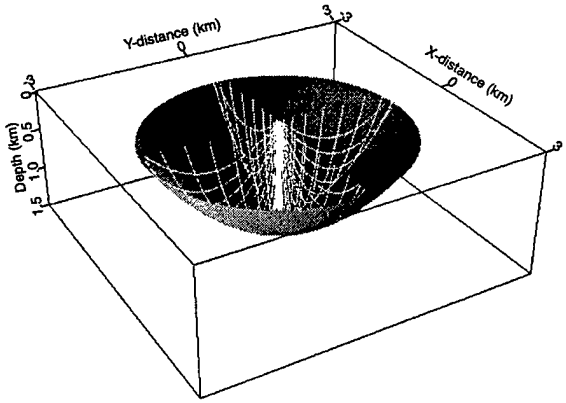

Figure 4. The rays(white) of linear sloth model have a parabolic shape. The grey surface is the caustic surface of the ray equations for this model.

in between the pairs of existing rays in order to meet the criteria of size and shape of triangular plates on the wavefront. Fig 2-a illustrates the interpolation of a single new ray. The two ray endpoints and their propagation directions form two straight lines in $3D$. An "approximate" center can be defined as the midpoint of the line segment that connects the two straight lines at their points of shortest distance. This approximate center, along with the two ray ends at the old WF, form a fan and a circular curve connecting the two ray end points. The new ray position is then found along the dividing direction from the approximate center, and at its intersection with the circular curve. Other parameters along the new ray are interpolated linearly.

There are other alternative methods of interpolating new rays, such as the parameterization of a wavefront by a third-order polynomial (Vinje *et al.*, 1996). However, they require special treatment in the vicinity of caustic points, since only rays belonging to the same phase must be used to determine quantities of the new ray. Moreover, we do not use the curvature of the wavefront obtained from DRT for the interpolation to keep the problems of KRT and DRT separate. We have found this method very stable.

Grid interpolation

Another interpolation procedure in DRT is the estimation of ray data at the output grid points. This is our final goal of the ray tracing algorithm. We perform the grid interpolation within ray tubes, which are prism-shaped bodies bounded by three rays and the triangles that connect them on the two WFs. First the grid points falling into (or close to) each cell are found. Then, the traveltime can be estimated at the each grid point in a similar way to the interpolation procedure for new rays(see Fig 2-b). The approximate center is determined by the three rays with ray endpoints on any of the two WFs. The distances from each grid point to the approximate center and to the simulated wavefront are calculated. The traveltime at the grid point is then recorded as $t_0 + d/v$, with t_0 the time at the wavefront, d the distance of the grid point away from the wavefront, and v the velocity at the grid point.

The above procedure is not suitable for interpolation of amplitude, because the isochrons surface is usually not the iso-amplitude surface. Here, we apply linear interpolation for amplitudes, which is based on the assumption that the amplitudes vary only slowly; otherwise, the validity conditions of the underlying asymptotic theory would be violated. Since the ray Jacobian—the determinant of Q in (4)—is proportional to the cross sectional area of the ray tube, we interpolate the ray Jacobian linearly with respect to the triangle areas on the two wavefronts.

Another parameter that requires interpolation at every grid point is the initial shooting direction, i.e., the initial take-off angles of the ray that would reach the grid point if the ray actually had been traced. This parameter is stored in order to distinguish between arrivals because two arrivals at a grid point cannot have almost equal take-off angles.

Model representation

The smoothness of the velocity model representation is critical to the calculation of amplitudes. The integration of the DRT system (4) requires continuity of the velocity field up to the second derivatives. Many ray tracing procedures (Farra, 1990) involve a type of spline interpolation for the evaluation of velocities at arbitrary points. Spline interpolation, however, is a time consuming procedure. Here, we define the velocity model on a fine grid (about three or four grid points per shortest significant model wavelength) and pre-calculate its first and second derivatives at all grid points by finite differences of second order. For the evaluation of the velocities and their derivatives at arbitrary points we use linear interpola-

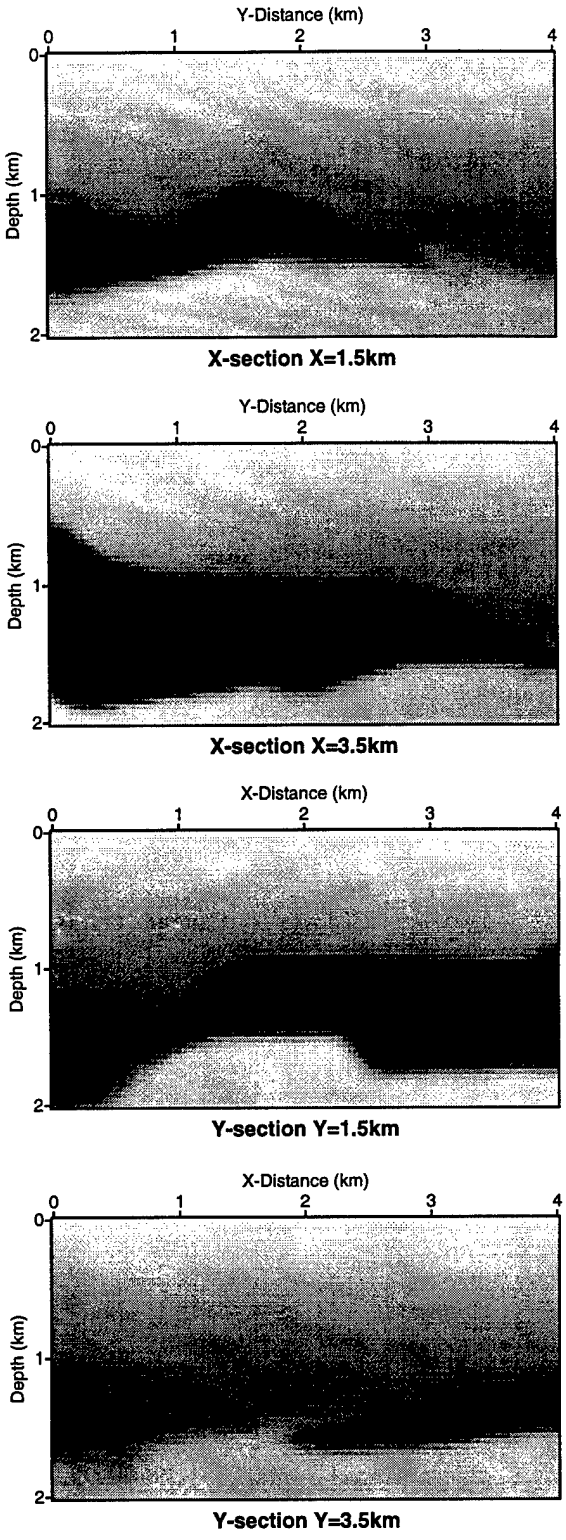

Figure 5. Four cross sections of the $3D$ SEG saltdome velocity model (subsection) at $x = 1.5km, x = 3.5km, y = 1.5km$, and $y = 3.5km$.

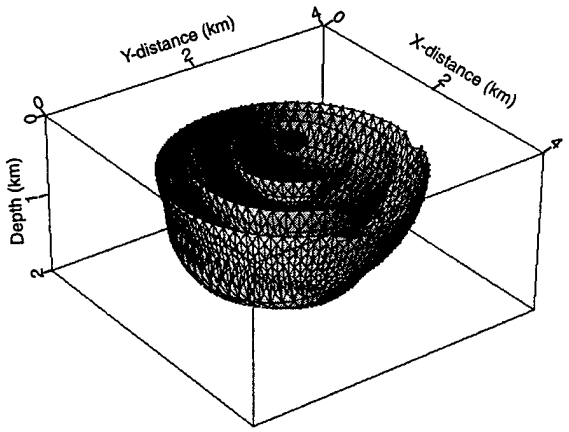

Figure 6. Triangulated wavefronts for smoothed salt dome model at $t = 0.1, 0.4, 0.65$, and $0.9s$. The source is located at the center of the up surface.

tion. For the smooth models defined on fine grids, the difference between this linear representation and a spline representation of the model is negligible.

When the considered model contains discontinuous velocities, a smoothing procedure must be applied to guarantee that the velocities vary smoothly. For the sake of computational efficiency, the interface conditions are eliminated here by using proper smoothing and a densely sampled grid model.

Examples

The first example provides a test of the accuracy of this modeling technique. The synthetic model we choose for this test is the one with constant gradient of squared slowness, i.e.,

$$\frac{1}{v^2(\mathbf{x})} = \frac{1}{v_0^2} + B_1 x_1 + B_2 x_2 + B_3 x_3. \qquad (12)$$

In such a medium, the rays have a parabolic shape; both traveltime and amplitude field can be expressed exactly by analytical solutions for comparison purposes. Figure 3 shows the $3D$ wave field with the gradient constants being $(0, 0, -0.2)s^2/km^3$. The relative difference of computed traveltimes and analytic ones is less than 0.1% through the whole interest area, while the differences between computed and analytical amplitudes are no more than 1%. The grey part in Fig 3 is the shadow zone, where no rays are entered. This is due to the negative gradient constant of B_3, which is equivalent to the increasing velocity with depth. In Figure 4, the grey surface is the caustic surface of the ray equations. It is the envelope of the parabolic rays.

The aim of the second example is to prove that our tracing algorithm can operate on a complex velocity model. This example is performed on a $3D$ SEG saltdome velocity model. This synthetic velocity model contains one complex salt dome with high velocity in the dome and low and slowly varying lateral layers outside the salt dome. Due to the RAM capacity of the computer, we extracted a subsection of the original model, which has part of the salt in the middle. The strong velocity contrast at the salt wall has violated the smoothness requirement of ray tracing, therefore we first smoothed this reference model. Figure 5 shows four cross sections of the smoothed velocity model. The grid size is $40m \times 40m \times 40m$. Figure 6 shows some wavefronts for this model. The wavefronts expand and become more complex for the later traveltimes. However, by using the wavefront construction technique, all the wavefronts have sufficient ray density. Figure 7 presents cross sections of traveltime maps of the above smoothed velocity model. The isochrons are spherical-like at the shallow parts, but the shape changes due to the salt in the middle depth.

Conclusions

We have demonstrated that numerically solving the ray equations on a smooth gridded model provides forward modeling that is fast enough for three-dimensional computations. Both the traveltimes and amplitudes proved to be smooth and stable in our examples. It remains to check the numerical accuracy of this technique, as compared to analytical solutions and alternative numerical methods. However, it is already known that the tetrahedral-based approach produces unacceptable amplitudes, due to the difficulty in efficiently obtaining accurate amplitudes across the internal interfaces.

The WFC procedure based on proper interpolation of new rays makes the dynamic ray tracing more efficient and results in a dense and consistent ray coverage throughout the model, even in areas of large geometrical spreading. When accurate amplitudes are required, we believe that this is a competitive method for development of ray theoretic wavefields.

Acknowledgments

The authors wish to acknowledge the support for this project given by the Office of Naval Research, Ocean Acoustics, grant number N00014-95-1-0508. Partial support was also provided by the Sponsors of the Consortium at the Center for Wave Phenomena, Colorado School of Mines.

References

Bleistein, N. 1984. *Mathematical Methods for Wave Phenomena.* Academic Press, Inc. Page 275.

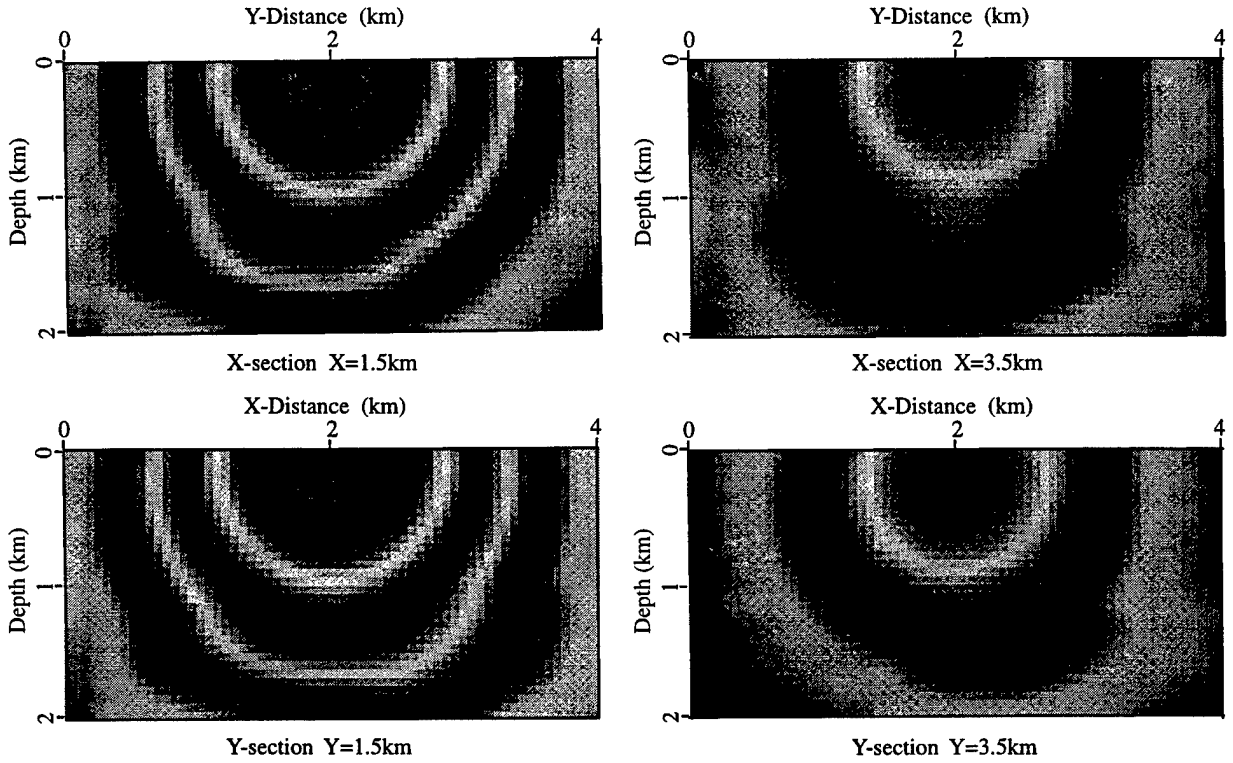

Figure 7. Cross sections of traveltime maps of the $3D$ salt dome model. The source is at $x = 2km, y = 2km, z = 0km$.

Bleistein, N., Cohen, J.K., & Hagin, F.G. 1987. Two and one-half dimensional born inversion with an arbitrary reference. *Geophysics*, **52**(1), 26–36.

Bleistein, N., Cohen, J. K., & Stockwell, Jr., J. W. 1996. *Mathematics of Multidimensional Seismic Inversion.* Colorado School of Mines.

Červený, V. 1987. Ray tracing algorithms in three-dimensional latrally varying layered structures. *Nolet, G., Ed., Seismic Tomography*, 99–133.

Červený, V. 1995. *Seismic Waves Fields in Three-Dimensional Isotropic and Anisotropic Structures.* Trondheim,Norway: University of Trondheim.

Farra, V. 1990. Amplitude computation in heterogeneous media by ray perturbation theory: a finite element approach. *Geophys. J. Int.*, **103**, 341–354.

Körnig, M. 1995. Cell ray tracing for smooth, isotropic media: a new concept based on a generalized analytic solution. *Geophys. J. Int.*, **123**, 391–408.

Meng, Z., & Bleistein, N. 1997. Wavefront contruction (WF) ray tracing in tetrahedral models – application to 3-D traveltime and ray path computations. *67th Annual Internat. Mtg., Soc. Expl. Geophys., Expanded Abstracts*, **67**, 1734–1737.

Sun, Y. Clapp, R., & Biondi, B. 1995. Three dimensional dynamic ray tracing in complex geological structures. *SEP-93.*

Vidale, J. E. 1988. Finite-difference calculation of travel times. *Bull. Seismol. Soc. Am.*, **78**(6), 2062–2076.

Vinje, V., Iversen, E., Astebol, K., & Gjöystdal, H. 1996. Estimation of multivalued arrivals in $3D$ models using wavefront construction-Part I & II. *Geophysical Prospecting*, 44, 819–858.

Virieux, J., & Farra, V. 1991. Ray tracing in 3-D complex isotropic media: An analysis of the problem. *Geophysics*, **56**(12), 2057–2069.